Sensing of Surface Strain with Flexible Fiber Bragg Strain Gages

Jochen Maul and Tobias Kipp

HBM GmbH, Im Tiefen See 45, 64293 Darmstadt, Germany
Emails: jochen.maul@hbm.com, tobias.kipp@hbm.com

Chapter 4-6

4. Bragg Fiber Interrogation and Multiplexing

For telecommunication wavelengths around 1550nm, tuneable laser sources represent a good basis for interrogation of fiber Bragg gratings and fiber Bragg sensors. In the HBM interrogators ("optical recorders"), a semiconductor optical amplifier (SOA) is combined with a high-performance fiber Fabry Perot tuneable filter (FFP-TF, a technology from Micron Optics Inc.), with optical isolators and with a coupler to perform a unidirectional ring laser with a maximum tuning range between ~1450nm and ~1650nm. This combination unifies the advantages of high optical gain and broad bandwidth of the SOA with the wide tuning range and the high spectral selectivity of the FFP-TF (free spectral range >200nm).

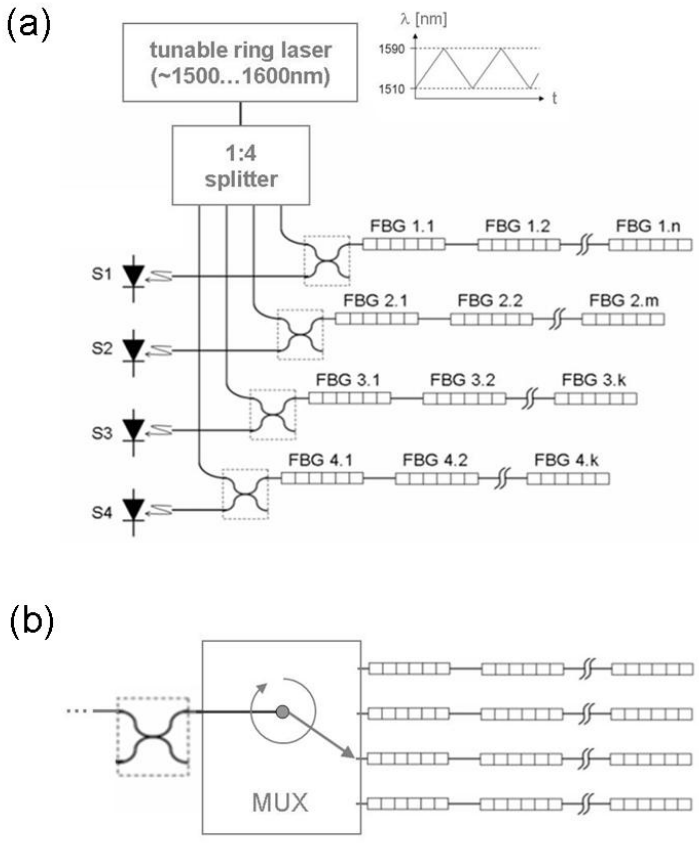

Fig. 3. (a) Scheme of an optical interrogator (4-channel model). Light from a tunable light source is split over 4 channels which couple light to up to 4 fibers with several fiber Bragg grating sensors (FBGs 1.1-4.k). The reflection spectrum of the FBGs is recorded by photodiodes (S1-S4). Dotted squares: Fiber couplers for back-reflected light from FBGs. **(b)** Symbolic scheme of an optical multiplexer ("MUX") channel with 1x4 multiplexing capability, connected with one interrogator output channel.

The principal setup of the interrogator is illustrated in **Fig. 3a**. The output of the tuned light source is split over (optionally up to) four optical fiber channels which are connected by one

Bragg sensor fiber each. In every chain, light reflected from the Bragg sensors is recorded by a photodiode which is connected via a fiber coupler. Here, the optical signal is converted into an electrical signal for further data processing. For dynamic interrogation, the FFP-TF is driven with scanning frequencies of up to 1 kHz (e.g. HBM dynamic interrogator DI 410). Whereas the accuracy for dynamic interrogation is not certified, static interrogators achieve 10pm wavelength accuracy and 1pm accuracy by implementation of a NIST certified acetylene gas reference cell (e.g. HBM static interrogator SI 401). All optical interrogators are equipped with either one (series DI/SI 1XX) or four (series DI/SI 4XX) fiber channels.

The number of sensors per chain is typically limited by both the spectral interrogating range (1510 nm – 1590 nm) and a reasonable minimum spectral distance of $\Delta\lambda_B$~5nm necessary to prevent mutual signal interference of two (spectrally) neighboring sensors after strain and temperature shift of the signal peak. Hence, a Bragg sensor chain with up to 15 Bragg sensors can be connected to each interrogator channel in principle. The standard HBM program is limited to 13 Bragg gratings per chain. For a 4-channel interrogator, the maximum number of sensors therefore amounts to 4x13=52.

The number of measuring channels can be increased by means of optical multiplexers, as sketched in **Fig. 3b**. The 4x8 and 4x16 multiplexers (HBM M408 and M416) for 4 optical input channels each use a network of 1x2 solid state all-crystal switches which allow fast non-mechanical electro-optical switching with a response time below 0.05 ms. Hence, the maximum number of Bragg sensors of the entire instrumentation in increased to 52x2=104, resp. to 52x4=208.

For dynamic interrogation, the usage of multiplexers however decreases the interrogation rate by a factor equalling the degree of multiplexing, i.e. from 1 kHz to 500Hz for 4x8 multiplexers and from 1 kHz to 250 Hz for 4x16 multiplexers. Furthermore, signal loss reduces the dynamic range to ~40dB for 4x8 multiplexing, resp. to ~30dB for 4x16 multiplexing.

5. HBM Fiber Bragg Sensors

a. Fiber-optical Strain Gages- Strain Measurement and Stress Analysis

In order to realize a fiber Bragg strain sensor, strain from the substrate needs to be fully transferred to the fiber Bragg grating. Therefore, the sensor needs to be tightly bonded onto the surface and the substrate strain has to be completely guided to the fiber. **Fig. 4a** shows the HBM strain sensor which is designed to enable ideal strain transfer into the glass fiber (HBM K-OL). This sensor allows to measure tension and compression without prestrain. The flexible material combination is chosen for sensing of high strain and to enable strain measurement even on bended surfaces, as it is demonstrated in the application example in **Fig. 4b.**

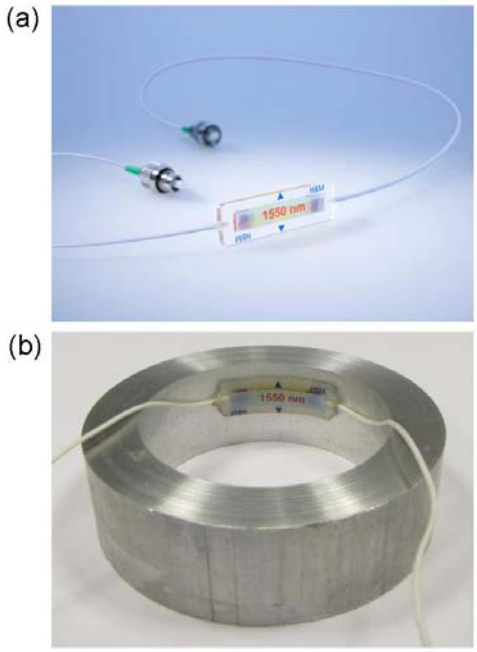

Fig. 4. (a) Optical linear strain gage (HBM K-OL) with two additional fiber connectors. (b) Optical linear strain gage installed onto a ring surface; inner radius = 35mm.

Some basic specifications of this K-OL optical strain gage ("OL") are shown in **Fig. 5**. It exhibits perfect linearity of the Bragg wavelength signal $\Delta\lambda_B/\lambda_B$ upon external strain (**Fig. 5a**). Here, the measured value of the *k* factor is close to the expected value (measured: k=0.78; theoretical: k=0.79; compare eqn. (12)). A continuous-operation test at ±5000µm/m alternating-load on a fiber reinforced plastic (GRP) spring demonstrates the capability of high strain measurement (**Fig. 5b**). The oscillation cycles were repeated 10^7 times, whereupon the full strain was also detected at the end of the cycle. The optical strain gage was also shown to record >±10.000µm/m in single bending tests.

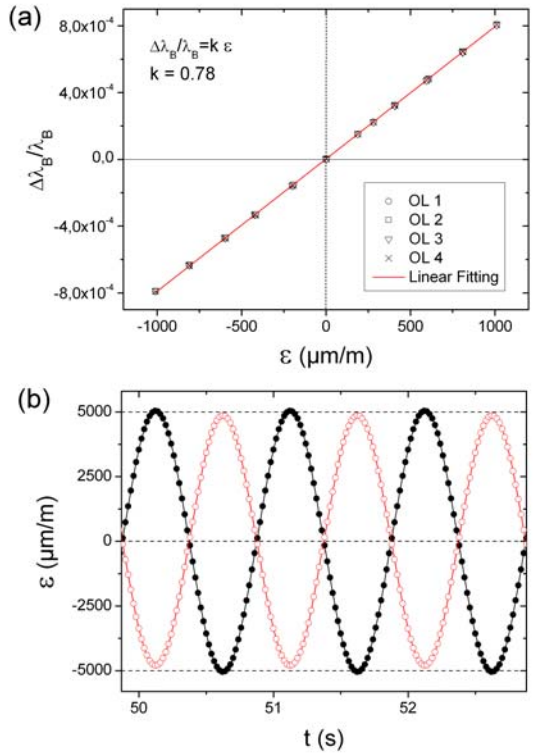

Fig. 5. (a) Linear strain response of optical strain gages ("OL") adhesively bonded on top of a calibrated stainless steel spring. (b) Strain response at ±5000µm/m strain level. Two optical strain gages are adhesively bonded on both sides of a oscillating glass fiber reinforced plastic (GRP) spring.

Since the fiber is guided within the optical strain sensor in a well defined way and tightly bonded onto the specimen surface, the expansion coefficient $\alpha_{\Lambda T}$ of the free fiber has to be

omitted for the bonded sensor. Instead, the thermal expansion coefficient of the specimen α_s has to be taken into account for the total strain signal

(15) $$\varepsilon = \varepsilon_m + \left(\alpha_{nT}/k + \alpha_s\right)\cdot \Delta T\,,$$

where ε_m is the mechanical strain applied to the specimen ($\varepsilon_m \equiv \Delta\varepsilon$ in eqn. 14).

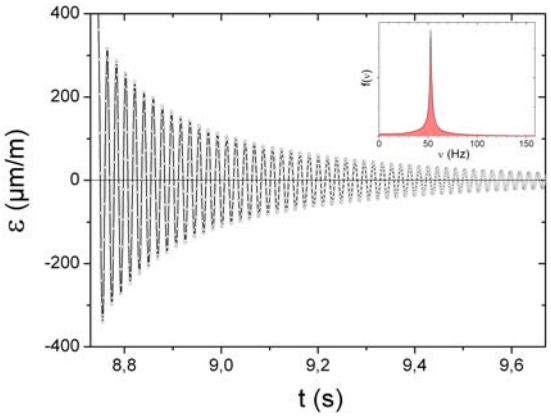

Fig. 6. Dynamic interrogation of a damped mechanical oscillation recorded by an optical strain gage adhesively bonded on top of an aluminium spring. Signal readout is performed by a dynamic interrogator (HBM DI410). The Fourier transform of the oscillation is given as inset.

An example for dynamic interrogation is given in **Fig. 6** where the damped oscillation of an aluminium spring was measured by an optical strain gage using a dynamic 1 kHz-interrogator (HBM DI 410). Here, the Fourier spectrum displays a center frequency around 50Hz and frequency contributions up to ~100Hz.

For two-dimensional strain measurements and subsequent stress analysis, a "rosette-type" optical strain gage ("OR" sensor) is available. Here, three Bragg gratings are inscribed within a sequence. The Bragg fiber is twice bend by 60° and embedded analogue to the linear optical strain sensor, as shown in **Fig. 7** (HBM K-OR).

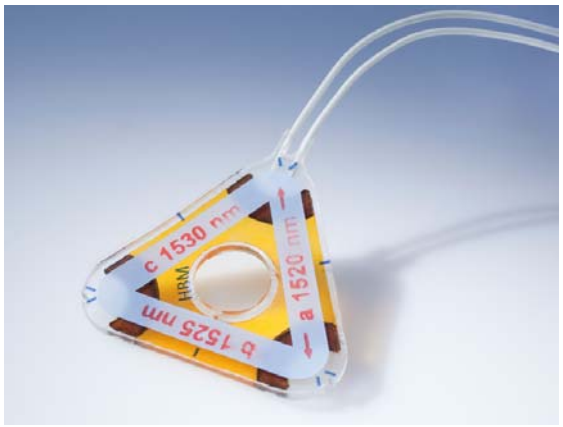

Fig. 7. Optical Rosette sensor with cover and label indicating Bragg wavelengths and clockwise grating arrangements (HBM K-OR).

From the measurement of the strain set $\{\varepsilon_a, \varepsilon_b, \varepsilon_c\}$, the two main normal stress components σ_1 and σ_2 are determined with this 0°/60°/120°- optical rosette sensor by [13]:

(16) $$\sigma_{1/2} = \frac{E}{1-\nu}\cdot\frac{\varepsilon_a+\varepsilon_b+\varepsilon_c}{3} \pm \frac{E}{1+\nu}\cdot\sqrt{\left(\frac{2\varepsilon_a-\varepsilon_b-\varepsilon_c}{3}\right)^2 + \frac{1}{3}\left(\varepsilon_b-\varepsilon_c\right)^2}$$

Here, E is the elastic modulus of the measurement body (e.g. E~66kN/mm^2 for Al and E~200kN/mm^2 for most steels) and ν is the inverse Poission ratio between transverse and longitudinal strain upon force in longitudinal direction (e.g., ν~0.33 for Al and ν~0.27 for

most steels). The angle φ (**Fig. 8b**) encloses the measuring grating *a* and the stress component σ_1 (see Ref. [13] for details).

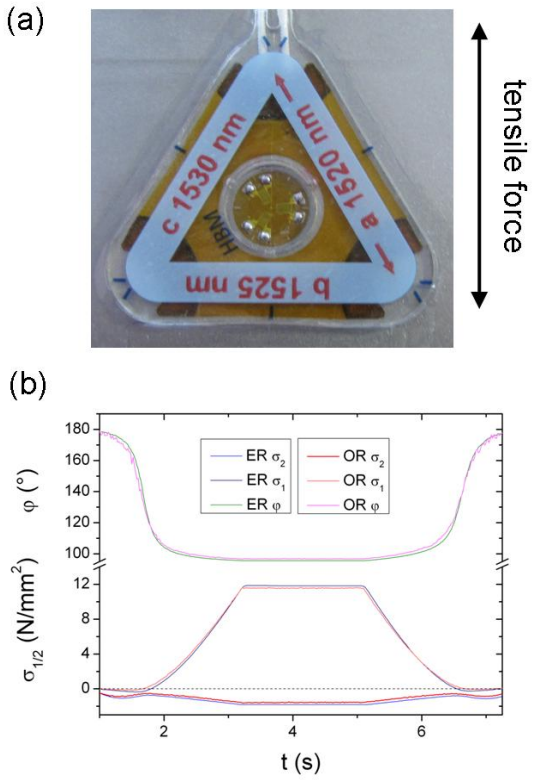

Fig. 8. (a) Measurement configuration to compare optical with electrical rosette strain gage. (b) Comparative stress analysis with optical rosette (OR) and electrical rosette (ER), both mounted on a aluminium tensile bar. The measurement gratings are denoted by "a,b,c". The diagram shows resulting main normal stress components σ_1 and σ_2, and the angle φ between σ_1 and grating *a*.

Fig. 8a shows a measurement configuration used to compare the optical rosette strain sensor with an electrical 0°/60°/120°-rosette strain sensor ("ER" sensor, type HBM RY73-6/120) which are bonded to an aluminium tensile bar. The two-dimensional strain measurements by both sensors are converted into the stress components σ_1, σ_2 and the angle φ as shown in **Fig. 8b.** Although the optical rosette sensor is larger than the electrical rosette sensor, both stress analyses yield well comparable results.

b. Temperature Compensation Gage

An important prerequisite for precise strain measurements using fiber Bragg sensors is an accurate compensation of any thermal influences. This is necessary since the influence of temperature amounts to a Bragg wavelength shift of $\alpha_T \approx 6.4\times10^{-6}/K$ which compares to a significant strain signal of $\alpha_T/k \approx 8.1$ µm/m/K.
Therefore, a temperature compensation element needs to be placed nearby the strain sensor.
In our approach, temperature compensation can be realized in two ways:

In case of a *known* uniaxial strain direction, a second optical strain gage is used for temperature compensation which is bonded perpendicular to the strain axis onto the specimen surface (**Fig. 9a**, left). Due to the low transverse strain sensitivity k_t of the optical strain gage compared to the longitudinal strain sensitivity k_l in fiber direction (k_t/k_l <10^{-3}), this gage almost exclusively measures the signal from temperature T and from the transverse contraction of the substrate material which amounts to $\nu \cdot k_l \cdot \varepsilon$. In particular, it exhibits the same temperature characteristics as the optical strain gage bonded in strain direction, i.e. it implies the same temporal temperature response as the original optical strain gage.

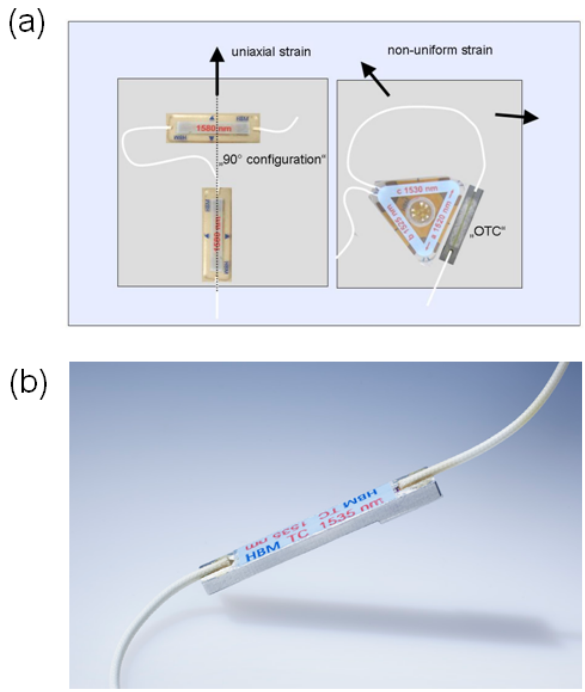

Fig. 9. (a) Temperature compensation with optical strain gage perpendicular to the known uniaxial strain direction (left), and with the OTC sensor in the presence of arbitrary non-uniform strain (right). (b) Optical temperature compensation sensor (HBM K-OTC).

In the presence of an *unknown* strain profile, this procedure is however not applicable. Here, the temperature measurement needs to be completely decoupled from any mechanical specimen strain. In our approach, a special optical temperature compensation ("OTC") gage is therefore designed: The Bragg fiber is mounted on top of an aluminium body which spatially decouples specimen strain from the Bragg grating. The apparent advantage of this sensor is the applicability for any strain profile, but the temperature signal is slightly retarded because of the finite heat capacity of the sensor body. For the compensation sensor, a time constant of τ~10s for the temperature response upon sudden temperature change at the specimen has to be considered. For comparable temperature conditions, the OTC sensor normally needs to be installed next to the Bragg grating of the optical strain gage, but its alignment angle relative to it is arbitrary (**Fig. 9a**, right).
Both accesses for temperature compensation are demonstrated in **Fig. 9a**; an enlarged view of the optical temperature compensation ("OTC") gage is shown in **Fig. 9b**.

Two central specifications of the OTC gage are obtained from **Fig. 10**. **Fig. 10a** shows a repeated temperature cycle in the operation range between -10°C and 80°C, which is measured as thermal strain by an optical strain gage. The corresponding OTC signal is used for temperature compensation. The temperature compensated signal ε' of the optical strain gage (K-OL resp. K-OR) is therefore given by:

$$\varepsilon' = \varepsilon(OL) - \varepsilon(OTC)\cdot\alpha(specimen)/\alpha(OTC) \qquad (17)$$
$$\varepsilon' = \varepsilon(OR) - \varepsilon(OTC)\cdot\alpha(specimen)/\alpha(OTC)$$

Here, $\alpha(OTC) = 30.6\mu m/m/K$. No mechanical strain is applied such that the pure temperature effect is filtered out. Even at the edge values of the temperature range, the compensation error is below 1%.

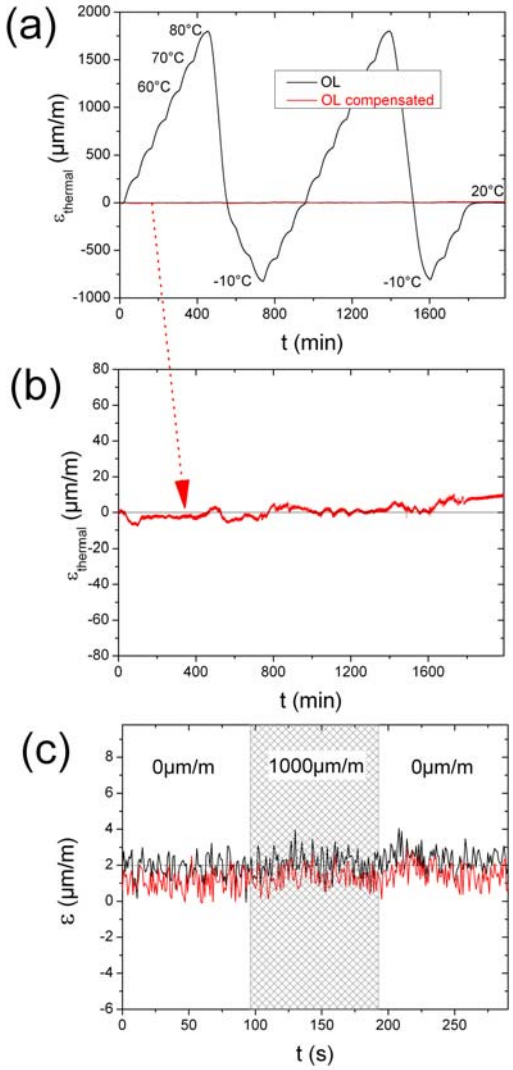

Fig. 10. (a) Temperature strain signal of an optical linear strain gage (OL), bonded on an aluminium body and exposed to several temperature cycles in a climate chamber, and corresponding signal after temperature compensation with an OTC gage. (b) Enlarged view: Temperature compensated OL signal. (c) Response of two OTC sensors upon a mechanical strain cycle applied to the substrate

The absolute compensation error in the complete temperature cycle is below 10µm/m (**Fig. 10b**). In addition, the OTC sensor design effectively decouples mechanical strain from the substrate as shown in **Fig. 10c**. Stretching of the substrate by 1000µm/m evidently effects no change in the OTC signal.

.

Fig. 11 illustrates a combined temperature and strain test where one optical strain gage is bonded on a steel body (α_s=10.8µm/m/K) and temperature compensation is realized with an OTC sensor. Temperature varies irregularly between ~20°C and ~80°C, and two individual mechanical strain events are carried out. The temperature compensated signal basically shows the two mechanical strain signals and a low background from temperature influences (<40µm/m). In this practical test, the time constants for temperature changes occasionally went significantly below τ=10s and therefore lead to a partly enhanced compensation error.

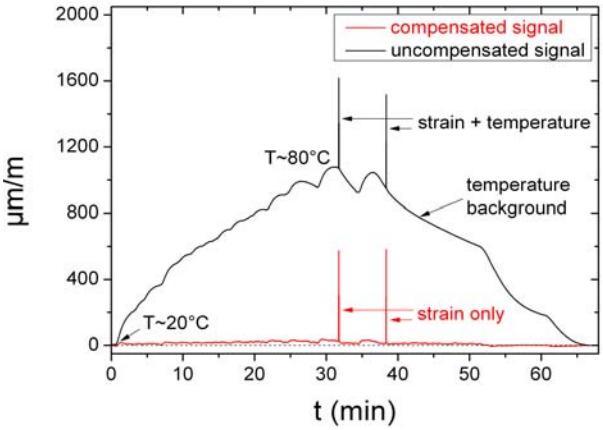

Fig. 11. Temperature compensation test in the presence of mechanical strain. The OL strain sensor was bonded on a steel body and temperature compensation was performed with an OTC gage.

6. Measurement Chain

Fig. 12. shows the Bragg spectrum of a measurement chain example containing 13 Bragg sensors, each adjacent sensor pair separated by a spectral distance of ~5nm. With this spectral distance, strain up to $\pm \Delta\lambda_B/\lambda_B/k$ ~±5nm/1550nm/0.78~±4000µm/m can be measured provided that the neighboring sensors are unstrained.

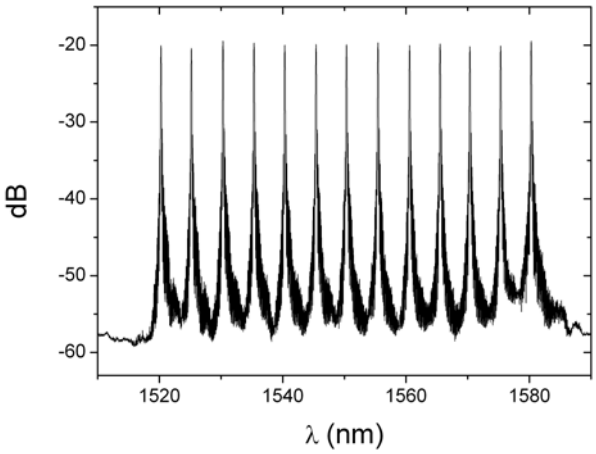

Fig. 12. Optical measurement chain with 13 Bragg gratings separated by a Bragg wavelength difference of 5nm each. The spatial distance between each pair of Bragg gratings is ~50cm.

Measurement chains are connected to the interrogator by means of FC/APC connectors with ends cut in a 8° angle. This prevents backreflection of signal background into the incoming interrogator fiber by exceeding the total reflection angle.

In practice, Bragg sensors are often separated by different fiber lengths connecting various installation spots. Thereby, the sensor fiber has to be elongated by insertion of fiber parts using optical splices. However, optical losses should be kept below 4dB within the sensor chain in order to avoid ambiguity in Bragg peak detection. This occurs especially when sidebands which are oftentimes up to 4dB below the corresponding Bragg peak level reach similar intensities as other Bragg peaks in the same chain.

Optical losses appear at different levels as it is summarized in **Fig. 13**: Whereas the specific loss of the connection fiber (telecommunication fiber) used to connect the interrogator with the sensor chain is as low as 0.2dB/km (one way), the specific loss of the sensor fiber is 9dB/km (one way). Therefore, the total length of the sensor fiber should not exceed ~200m. However, the length of the connection fiber is not critical because it introduces an overall signal damping of *all* Bragg sensors.

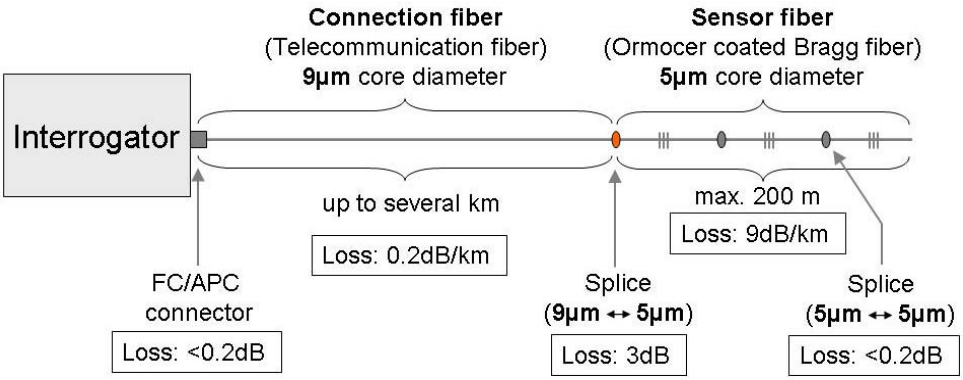

Fig. 13. Recommended limits in fiber lengths combinations for the measurement chain with acceptable signal damping.

Due to optical mode field adaption from the sensor fiber (core diameter ~5µm) to the low-loss telecommunication fiber (core diameter ~9µm), bidirectional optical losses amount to ~3dB for each splice between both fiber types. Therefore, the complete chain should not contain more than one interconnection splice, i.e. fiber types should not be changed more than once per chain. The process of fiber splicing is briefly illustrated in **Fig. 14**. Thereby both fiber ends are cut in an 0° angle, then precisely aligned and finally fused by an electrical arc discharge. Splices between the same fiber types only introduce losses typically below ~0.2dB (one way).

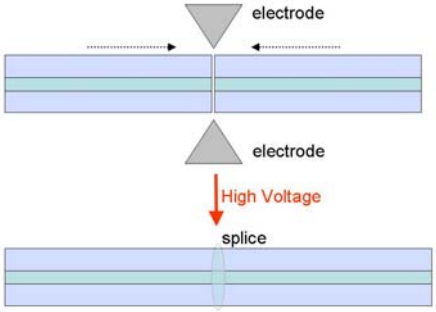

Fig. 14. Process of fiber splicing by electrical arc discharge.

Another source of optical losses is related to critical fiber bending. In this case, the total reflection angle is under-run and light escapes from the fiber core. The critical bending radius is as low as 2 mm for the sensor fiber, but ~20 mm for the telecommunication fiber.

For accurate detection of the Bragg wavelengths, fiber bending and fiber positioning should not be changed too much during the measurement process: The interrogators of the HBM SI/DI series utilize linearly polarized light which may change orientation during fiber bending. Since the Bragg gratings commonly show some rotational anisotropy, changing the polarization state of light used for interrogation leads to a small polarization shift of the Bragg wavelength up to ~20pm. It is therefore recommended to fix the complete chain at selected locations once all sensors are installed.

Finally, a time-of-flight (TOF) correction for the light travelling time can be implemented for long connection fibers: since the DI/SI interrogators rely on a scanning technique, the wavelength scanning time is directly translated into a proportional scanning wavelength at the data acquisition side. Therefore, any additional propagation time of the Bragg signal from the grating to the photodiode due to optical pathways leads to an artificial shift in the detection wavelength. For example, with a speed of light of $c_0/n \sim 2*10^8$ m/s ($c_0=3*10^8$ m/s is the speed

of light in air, n~1.5 is the fiber refractive index), light needs ~5ns to pass 1m fiber. The TOF shift becomes especially critical for dynamic interrogation. In case of 1 kHz interrogators, the scanning time for the wavelength range of 80nm amounts to ~0.4ms. For kilometer long connection fibers, the TOF shift can easily reach values in the nm regime which have to be considered for absolute measurements.

References

[1] Ch.K. Kao, Optical fiber technology, IEEE Press, New York, USA (1981);
The Nobel Prize in Physics 2009 – Press Release, Nobel Foundation, http://nobelprize.org/nobel_prizes/physics/laureates/2009/press.html;

[2] P.S. Theocaris, Moiré fringes in strain analysis, Pergamon (1969).

[3] R.P. Khetan and F.P. Chiang, Strain analysis by one-beam laser speckle interferometry, Appl. Opt. 15, 2205-2215 (1976).

[4] C. Belleville and G. Duplain, White-light interferometric multimode fiber-optic strain sensor, Opt. Lett. 18, 78-80 (1993).

[5] P.B. Tarsa, M. Brzozowski, P. Rabinowitz, and K.K. Lehmann, Cavity ringdown strain gauge, Opt. Lett. 29, 1339-1341 (2004).

[6] D. Graham-Rowe, Sensors take the strain, Nat. Photon. 1, 307-309 (2007).

[7] K.O. Hill, Y. Fujii, D. C. Johnson, and B. S. Kawasaki, Photosensitivity in optical fiber waveguides: application to reflection fiber fabrication, Appl. Phys. Lett. 32, 647-649 (1978).

[8] G. Meltz, W.W. Morey, and W.H. Glenn, Formation of Bragg gratings in optical fibers by a transverse holographic method, Opt. Lett. 14, 823-825 (1989).

[9] E. Brinkmeyer, „Faseroptische Gitter“, in: Optische Kommunikationstechnik, Eds. E. Voges and K. Petermann, Springer (2002).

[10] M.W. Rothhardt, C. Chojetzki, and H.R. Müller, High-mechanical-strength single-pulse draw tower gratings, Proc. SPIE 5579, 127 (2004).

[11] M. Kreuzer, Strain Measurement with Fiber Bragg Grating Sensors (2007), online at www.hbm.com .

[12] A. Bertholds and R. Dändliker, Determination of the individual strain optic coefficients in single mode optical fibers, J. Lightwave Tech. 6, 17-20 (1988).

[13] K. Hoffmann, An Introduction to Measurements using Strain Gages, HBM (1987).

[14] J. Zhao, X. Zhang, Y. Huang, and X. Ren, Experimental analysis of birefringence effects on fiber Bragg gratings induced by lateral compression, Opt. Commun. 229, 203-207 (2004).

[15] W. Lee, J. Lee, C. Henderson, H.F. Taylor, R. James, C.E. Lee, V. Swenson, R.A. Atkins, and W.G. Gemeiner, Railroad bridge instrumentation with fiber-optic sensors, Appl. Opt. 38, 1110-1114 (1999).